MODELING SCATTERED INTENSITIES FOR MULTIPLE PARTICLE TIRM USING MIE THEORY

A Thesis

by

ADAM L. ALLEN

Submitted to the Office of Graduate Studies of
Texas A&M University
in partial fulfillment of the requirements for the degree of

MASTER OF SCIENCE

August 2006

Major Subject: Biomedical Engineering

MODELING SCATTERED INTENSITIES FOR MULTIPLE PARTICLE TIRM USING MIE THEORY

A Thesis

by

ADAM L. ALLEN

Submitted to the Office of Graduate Studies of
Texas A&M University
in partial fulfillment of the requirements for the degree of

MASTER OF SCIENCE

Approved by:

Chair of Committee,	Kenith Meissner
Committee Members,	Michael A. Bevan
	Gerard L. Coté
Head of Department,	Gerard L. Coté

August 2006

Major Subject: Biomedical Engineering

ABSTRACT

Modeling Scattered Intensities for Multiple Particle TIRM

Using Mie Theory. (August 2006)

Adam L. Allen, B.S., Texas A&M University

Chair of Advisory Committee: Dr. Kenith Meissner

Single particle TIRM experiments measure particle-surface separation distance by tracking scattered intensities. The scattered light is generated by an evanescent wave interacting with a levitating microsphere. The exponential decay of the evanescent wave, normal to the surface, results in scattered intensities that vary with separation distance. Measurement of the separation distance allows us to calculate the total potential energy profile acting on the particles. These experiments have been shown to exhibit nanometer spatial resolution and the ability to detect potentials on the order of kT with no external treatment of the particle. We find that the separation distance is a function of the decay of the evanescent wave and the size of the sphere. Different sizes of spheres, located the same distance from the surface, exhibit varying scattered intensity distributions.

Single particles have been studied extensively but multiple particle experiments are needed for studies of more complex systems and surfaces. Increasing the number of colloidal particles in a TIRM experiment greatly increases the complexity of the system. Calculation of separation distances and potentials over a large group of microspheres requires that the spheres display a uniform stuck-particle intensity distribution. But, for large numbers of particles, this is not the case. In some instances, stuck-particle intensities can vary more than an order of magnitude.

This research involves creating a mathematical model to study scattered intensity distributions for a large size range of polystyrene microspheres. The model is based on basic Mie theory. We compare the theoretically simulated results to the experimentally obtained results and find that scattered intensity variations in multiple particle TIRM experiments are attributed to particle polydispersity (particle size variation). This is a very important result because we know that if we can maintain a relatively uniform particle size distribution, then we will see a relatively uniform stuck-particle intensity distribution. The model can then be used to select a size range of microspheres that will exhibit a more uniform distribution so as to increase the sensitivity and feasibility of multiple particle TIRM.

TABLE OF CONTENTS

Page

LIST OF FIGURES

INTRODUCTION

A novel technique, called total internal reflection microscopy (TIRM), has been developed that can measure distances as small as a nanometer. TIRM is special because it provides a very sensitive, non-intrusive and instantaneous[1] ability to measure these extremely small distances. In TIRM we track the intensity of light scattered by a very small sphere. Changes in this scattered intensity represent a change in distance between the sphere and a transparent plate. This allows for us to physically observe, in real-time, the changes in scattered intensity; as a result, using a microscope, we can see these differences in distance. This is true even though we can measure distances that are approximately 20,000 times smaller than the width of human hair.

TIRM is also useful because we can use these measured distances to calculate the total sum of forces, or potential energies, acting on the sphere. Since we can detect very small changes in distance and we use this information to calculate the forces acting on the sphere, we can detect forces with unprecedented sensitivity. It has been shown that TIRM is able to detect forces on the order of $k_B T$ [1]. There are many interesting chemical and biomedical applications because of the extreme sensitivity.

Dr. Bevan's group at Texas A&M University is interested in using this technology to map the potential profiles of patterned surface. Instead of using single sphere, this technique makes use of a large number of small spheres to track changes in distance. If these spheres are spread out over a patterned surface, we measure the surface variations. Then, using these measured distances, we can calculate the potential energy variations across the surface.

This thesis follows the style of Optics Letters.

In TIRM the scattered light is generated by an evanescent wave interacting with a sphere that is suspended in water. The evanescent wave decays exponentially as distance from the surface increases. So, the scattered intensity will decrease as distance from the surface increases. We see that once the scattered intensity is measured, the separation distance between the sphere and the surface is a function of the decay of the evanescent wave. But, we will see that if we use multiple spherical particles the scattered intensities vary greatly for spheres attached to the surface (i.e., at the same distance).

This research looked to describe the differences in scattered intensity values observed in TIRM using multiple particles. We created a model using basic Mie scattering theory to describe scattered intensity values of a large range of sphere diameters. The model calculates the angular scattered intensity values for parameters defined experimentally. We then compared the theoretically calculated intensities to the experimentally measured intensities. We show that the scattered intensity variations are attributed to the polydispersity, or size variation, of the spheres used experimentally. Using this information we can choose a size range of spheres that will exhibit a more uniform intensity distribution and will make multiple particle TIRM experiments, such as Dr. Bevan's new technique, more practical and useful.

PROBLEM: SCATTERED INTENSITY VARIATIONS IN TIRM

Total internal reflection microscopy (TIRM). In the late 1980's TIRM was developed as a novel technique used to measure particle surface-interactions[1]. Single particle TIRM experiments measure particle-surface separation distance by tracking scattered intensities. The scattered light is generated by evanescent wave interaction with a levitating particle. The exponential decay of the evanescent wave normal to the surface results in scattered intensities that vary with particle-surface separation distance. This scattered intensity is also a function of the particle size. Different sizes of particles, located the same distance from the surface, exhibit different scattered intensity distributions. For single particle experiments, size variation does not play a significant role in separation distance calculations. Later on, we will see how polydispersity creates problems in multiple particle TIRM systems.

Evanescent wave generation. As the name suggests, TIRM relies on the principle of total reflection. Snell's law tells us that if a wave, traveling in medium #1 (with refractive index m_1), is incident on medium #2 (with refractive index m_2) where $m_2 < m_1$, part of the wave is reflected back into medium #1 (Figure 1). At a particular angle, the wave is totally reflected. This is known as the critical angle and is given by the relationship[4]:

$$\theta_c = \sin^{-1}\left(\frac{m_2}{m_1}\right) \tag{1}$$

Incidence at any angle greater than or equal to the critical angle will result in total reflection. Although, it is impossible to have complete reflection of the wave, even at

incident angles greater than the critical angle[2]. In this situation, a surface wave, or evanescent (EV) wave, is produced.

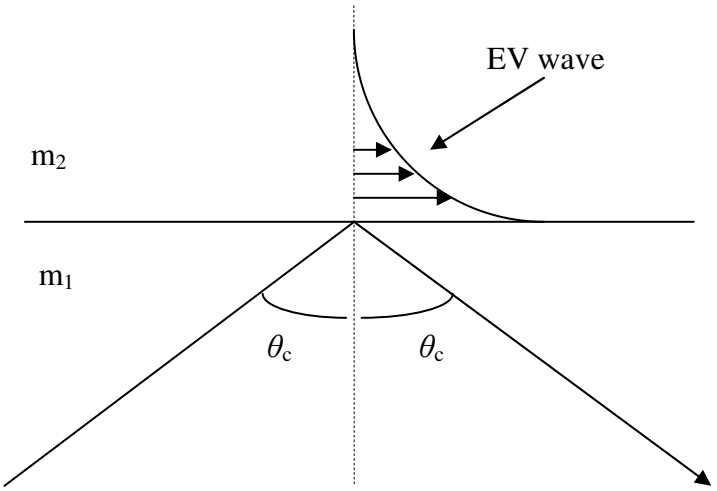

Fig. 1. Evanescent wave generation with refractive indices, $m_1 > m_2$.

The EV wave travels in medium #2 along the boundary and in the direction of the incident wave. In medium #2, the EV wave is attenuated exponentially normal to the boundary. The relationship can be described by [1, 3]:

$$I(h) = I_0 \cdot \exp(-\beta h) \tag{2}$$

The value of I_0, or the intensity of the particle stuck to the surface (at h=0), is very important in TIRM experiments and will be discussed in more detail later in this section. We can then calculate the scattered intensity of the EV wave at a distance h from the boundary using the intensity directly behind the boundary interface, I_0, and the EV wave decay length, β:

$$\beta = \frac{4\pi}{\lambda}\sqrt{(m_1 \sin(\theta_1))^2 - m_2^2} \tag{3}$$

Single particle TIRM. The 1st step in TIRM experiments is to establish the value of I_0 (eq. (2)). For TIRM experiments, we can define this value as the baseline intensity or the "stuck-particle" intensity. It is measured by physically attaching the microsphere to the surface of the slide and performing a TIRM study. For microspheres of polystyrene or glass, gravitational effects cause the spheres, which are denser than water, to come in contact with the glass slide[1]. Since the particle is attached to the surface of the glass slide (h = 0), the measured scattered intensity is not a function of separation distance but is denoted as the baseline intensity, I_0. As we will see, the stuck-particle intensity is highly dependent on the size of the particle. This becomes a major problem in multiple particle experiments and will be discussed in further detail.

Once I_0 is established, the system involves suspending a microsphere in an aqueous solution on top of a glass slide. An electrostatic charge is placed on the glass slide and on the particles to overcome gravitational effects so that the particles levitate[1]. Incident light from a laser is directed at an angle greater than or equal to the critical angle so that an EV wave is produced at the interface between the glass slide and the aqueous solution (Figure 2). The microsphere scatters the light from the EV wave. The scattered intensity is directly related to the intensity of the EV wave and the size of the particle. As we know, the EV wave decays exponentially with distance from the glass slide. Consequently, we can use the scattered intensity from the microsphere to directly measure how far the microsphere is from the glass slide by using equation (2). A thorough description of the process is described by Dennis C. Prieve[1].

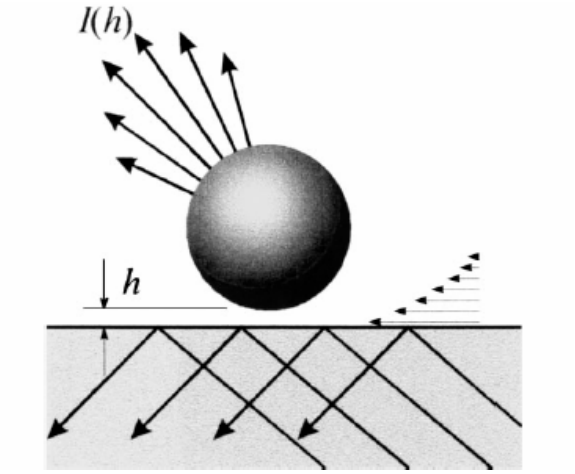

Fig. 2. Basic set up for TIRM[1]

Mapping potential energies. Dr. Bevan's group has been focused on using TIRM to map potential energy profiles of the particle-surface interaction. The technique has been shown to exhibit sensitivity to potentials on the order of k_BT, more than two orders of magnitude more sensitive than atomic force microscopy (AFM)[4]. This technique is extremely sensitive because it utilizes Brownian motion to detect changes in potential energy.

In order to maintain a levitated state there are three potential energies acting on the particle: gravitational, electrostatic, and van der Waals forces. The sum of these forces represents the total potential energy profile for the particle. While in this levitated state, Brownian motion continuously causes variations in the particle-surface separation (Figure 3).

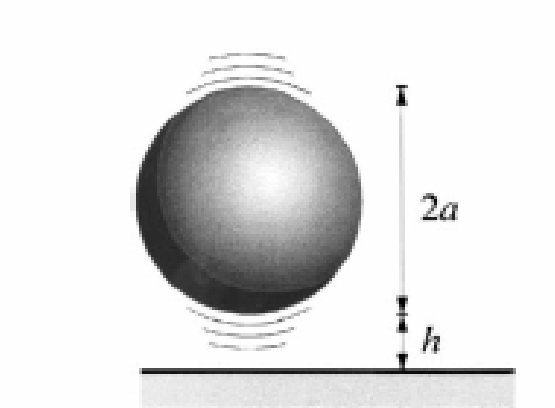

Fig. 3. Brownian motion continuously affects the levitating particle[1]

If we know the potentials acting on the particle, we can know the probability of finding the particle at a certain separation distance[1].

$$p(h) = A \cdot \exp\left(-\frac{\phi(h)}{k_B T}\right) \tag{4}$$

Where k_B is Boltzmann's constant, A is a normalization constant due to the number height observations, $p(h)$ is the probability density of heights sampled and $\varphi(h)$ represents the total potential energy profile for the particle. If a large number of observations are used, a time-dependent height histogram will be a good approximation of $p(h)$. We can use this approximation to calculate an unknown total potential energy profile $\varphi(h)$ acting on the particle.

Multiple particle TIRM. Multiple particle TIRM studies have become more common and more useful as technology has continued to advance. Using an ensemble of colloidal particles, instead of a single particle, creates a much more complex system but results in systems that maintain high sensitivity but yield statistically significant results. Diffusing colloidal probe microscopy (DCPM) is one system that is being developed to map potential energy landscapes[4] of heterogeneous surfaces. It will be discussed more thoroughly later in this section.

As explained previously, TIRM measures particle-wall separation and potential energy (PE) profiles by tracking the scattered intensities of a colloidal particle excited by an evanescent wave. Thus, the separation distance and PE profiles are a function of 1) the evanescent decay normal to the surface and 2) the size of particle. Once the baseline intensity, I_0, is established for a single particle experiment, size is not a factor and does not significantly contribute to the measure of separation distance. But for multiple particle experiments, establishing the baseline is very difficult. The polydispersity of a larger number of particles causes scattered intensity variations. The polydispersity makes multiple particle TIRM calculations very complex. Ensemble averaging of particle intensities is required. This is not advantageous in achieving desired resolution and sensitivity.

There are different methods in which ensemble averages are measured. One common method utilizes scattering techniques to provide a descriptive result. Light scattering is very well established[5] but, depends heavily on the distribution characteristics of the particles and does not account for signal noise. Another method involves using optical microscopy to measure the equilibrium distribution functions of colloidal systems[6].

Diffusing colloidal probe microscopy (DCPM). A novel technique is being developed by Dr. Bevan's group at Texas A&M University that combines TIRM and video microscopy to map heterogeneous surfaces (Figure 4a). Known as Diffusing Colloidal Probe Microscopy (DCPM) the technique maps the potential energy profiles associated with the surface.

DCPM makes use of a large number of polystyrene or silica microspheres to map potential energy profiles (Figure 4b). We chose to focus our attention on polystyrene microspheres because they have more uniform and well-defined properties when compared to silica. Also, experimentally Dr. Bevan's group works with polystyrene more.

DCPM incorporates ensemble averaging to measure the total potential energy profiles of a large number of particles. Ensemble averaging is a technique that measures the height of the particle, h, relative to the most probable height of the particle, h_{m}. h_{m} is also referred to as the reference height, h_{ref}. As described previously, the time averaged height histogram is a good approximation for $n(h)$. Wu *et al*, published in *Langmuir* 2005, described the potential energy profile relative to the reference state can then be found from[4]:

$$\frac{\varphi(h)-\varphi(h_{ref})}{k_B T} = \ln\left[\frac{n(h_{ref})}{n(h)}\right] \tag{5}$$

In this paper, only 11 single particle averages were calculated. It was determined that "polydispersity is sufficiently small so that combining 11 single particle height histograms produces an average profile consistent with the average properties of the silica colloids"[4]. They also mention that precise ensemble averaging requires the wall to uniform and all particles to be uniform. The ensemble averaging technique can only get more precise if we are able to use microspheres that exhibit more uniform intensity distributions.

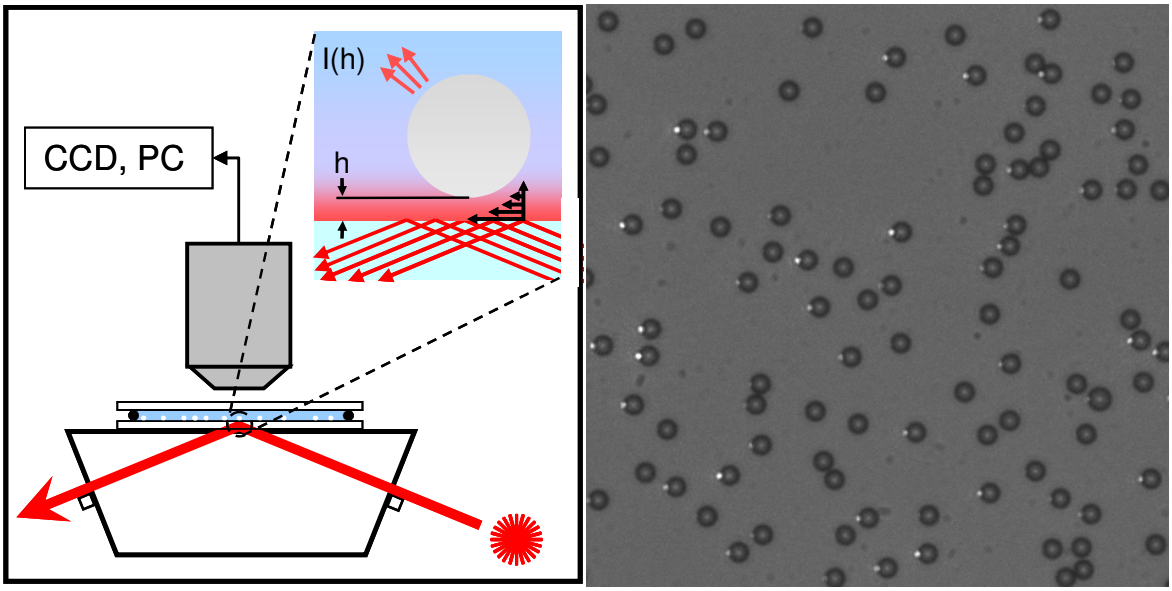

(a) (b)

Fig. 4. DCPM set up and results. (a) Schematic illustration of ensemble TIRM apparatus with laser, prism, batch cell, microscope, CCD camera, and data acquisition PC. Inset shows schematic representation of levitated particle scattering evanescent wave with intensity, *I(h)*, as a function of particle-wall surface separation, *h*. (b) CCD image from top view of levitated particles scattering evanescent wave (white spots) with transmitted light illuminating particles (dark rings).

SOLUTION: MIE THEORY

History of Mie theory. Mie theory, also called Lorenz-Mie theory, was independently developed and named for Gustav Mie[7] (1868 – 1957) and Ludvig Lorenz (1829 – 1891). It provides a complete mathematical theory for scattering by small particles. While Rayleigh scattering is concerned with particles that have a diameter to wavelength ratio much less than one, Mie encompasses all possible ratios. Applications include meteorological optics such as cloud or haze scattering, Doppler radar (scattering of radar energy by raindrops), and understanding the appearance of common materials including biological tissue.

Major books on the topic include *Absorption and Scattering of Light by Small Particles* by C.F. Bohren and D.R. Huffman[8] and *Light Scattering by Small Particles* by H.C. van de Hulst. A variety of other books and references are also available which provide a detailed analytical explanation of Mie theory for varying conditions and particle geometries.

The Bohren and Huffman book has been a standard reference for anyone studying Mie theory in the last 20 years. Even though it was first published in 1983, the description of Mie processes and calculation of Mie formulas is presented in a clear and unrivaled manner. Our research and resulting computer model rely heavily on the equations and assumptions presented in this book.

Spherical particles have been studied more extensively than any other particle. The interest in spheres is two fold: 1) that the symmetry has allowed for a Mie theory solution to be available[8] 2) that most small particles of interest, whether man made or naturally occurring, are spheres or can be approximated by spheres.

Assumptions in Mie theory. Mie theory for small particles is based on three major assumptions. First of all, the particles are assumed to be homogeneous and made of materials that are linear, isotropic, and optically linear. Secondly, each particle is assumed to be located in an infinite homogeneous, lossless medium. In other words, even when dealing with multiple particles, we assume single particle scattering. And lastly, it is assumed that the incident light is a continuous and infinite plane wave.

In order to model evanescent scattering using basic unmodified Mie theory, we must assume a strict set of parameters. Chew[3] *et al* defined these parameters as 1) the incident light must be perpendicularly polarized and 2) the scattering detection plane is located directly above the particle (i.e., at a scattering angle of 90º). In this case, the scattered wave will maintain perpendicular polarization and classic Mie theory will hold. In this case, the symmetry of the spherical vector harmonics is not destroyed by the exponential damping of the evanescent wave[3]. This assumption is crucial in allowing our model to give an accurate representation of scattered intensity values.

To model other scattering planes and polarizations, Mie theory must be expanded upon to model the evanescent wave instead of a plane wave. Evanescent wave interaction with microscopic spheres has been described using multi-pole expansion[3], geometric optics[9] and group-theory methods[10].

Angular scattered intensities. Modeling the interaction of a plane wave with a spherical particle is a very complex problem. The solution involves transforming the plane wave into vector spherical harmonics and is described extensively in Bohren and Huffman[8]. Using this transformation we are able to acquire a formula for the scattered electric field:

$$\mathbf{E}_{scatter} = E_0 \sum_{n=1}^{\infty} i^n \frac{2n+1}{n(n+1)} \left(i a_n \mathbf{N}_{e1n}^3 - b_n \mathbf{M}_{o1n}^3 \right) \tag{6}$$

Where, E_0 is the amplitude of the incident electric field and $\mathbf{M}_{01n}^{3}$ and $\mathbf{N}_{01n}^{3}$ are the vector spherical harmonics of the 3rd kind. a_n and b_n are the Mie scattered field expansion coefficients. A solution to this formula is found in Bohren and Huffman with equations for the a_n and b_n coefficients:

$$a_n = \frac{m^2 j_n(mx)[xj_n(x)]' - j_n(x)[mxj_n(mx)]'}{m^2 j_n(mx)[xh_n^{(1)}(x)]' - h_n^{(1)}(x)[mxj_n(mx)]'} \tag{7}$$

$$b_n = \frac{j_n(mx)[xj_n(x)]' - j_n(x)[mxj_n(mx)]'}{j_n(mx)[xh_n^{(1)}(x)]' - h_n^{(1)}(x)[mxj_n(mx)]'} \tag{8}$$

These coefficients are functions of the spherical Bessel and Hankel functions, j_n and $h_n^{(1)}$. The Bessel and Hankel function variables, x and m, are the two most important parameters in Mie theory calculations. x is defined as the size parameter of the particle where a is the particle radius (μm), λ is the wavelength of the incident light (nm) and m_{medium} is the refractive index of the medium surrounding the sphere. m is defined as the relative refractive index. The sensitivity to x and m will be discussed later in the the **Size effects** section. We compute a_n and b_n for a defined value of m and a specific size parameter, x.

$$x = \frac{2\pi a}{\lambda} m_{medium} \tag{9}$$

$$m = \frac{m_{sphere}}{m_{medium}} \tag{10}$$

Other functions that are important in studying scattered intensities are the functions π_n and τ_n. These functions are known as the angular eigenfunctions. They describe the angular scattering patterns of the vector spherical harmonics and are a function of the scattering angle, θ. These functions follow the recursive relationship:

$$\pi_n(\cos\theta) = \left[\frac{2n-1}{n-1}\cos(\theta)\cdot\pi_{n-1}\right] - \left[\frac{n}{n-1}\cdot\pi_{n-2}\right] \tag{11}$$

$$\tau_n(\cos\theta) = \left[n\cdot\cos(\theta)\cdot\pi_n\right] - \left[(n+1)\cdot\pi_{n-1}\right] \tag{12}$$

Where initial conditions are defined by,

$$\pi_0 = 0 \quad \pi_1 = 1 \quad \pi_2 = 3\cos(\theta)$$

$$\tau_0 = 0 \quad \tau_1 = \cos(\theta) \quad \tau_2 = 3\cos(2\cdot\theta)$$

We compute the angular scattering functions over the entire range of scattering angles, θ from 0 to 2π. Once the a_n, b_n, π_n and τ_n coefficients are calculated we can analyze the angular scattering amplitudes, S_1 and S_2, by the relationship:

$$S_1 = \sum_{n=1}^{n_{max}} \frac{2n+1}{n(n+1)}\left(a_n\pi_n + b_n\tau_n\right) \tag{13}$$

$$S_2 = \sum_{n=1}^{n_{max}} \frac{2n+1}{n(n+1)}\left(a_n\tau_n + b_n\pi_n\right) \tag{14}$$

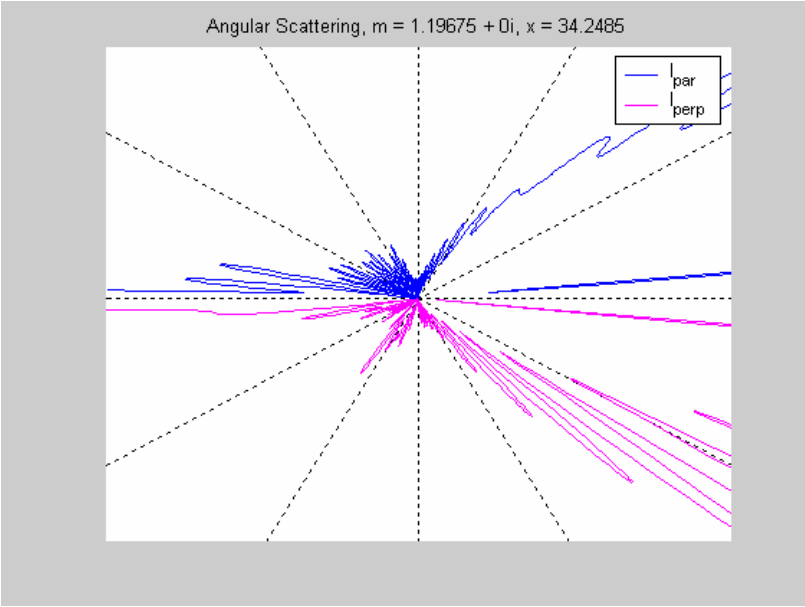

Fig. 5. Angular scattering polar plot. Angular plot of scattered intensities for a 4μm diameter polystyrene microsphere excited by 488 nm light.

The magnitudes of these functions, $|S_1|^2$ and $|S_2|^2$, represent the scattered irradiance per unit irradiance[11] for incident light that is perpendicular and parallel polarization, respectively (Figure 5).

If we then sum over all scattering directions, we obtain the scattering cross section of the particle, C_{sca}.

$$C_{sca} = \sum_{all\ \theta} \left(|S_1|^2 + |S_2|^2 \right) \tag{15}$$

The scattering cross-section can be thought of as the way that the sphere might look from the perspective of the incoming light. We can also find the scattering efficiency, Q_{sca}, by normalizing the scattering cross-section to the particle size parameter:

$$Q_{sca} = \frac{C_{sca}}{\pi\, x^2} \tag{16}$$

The scattering efficiency is often used as a way to observe scattering data over a range of size parameters.

From this point the scattered intensity values can be calculated fairly easily. Bohren and Huffman showed that given the scattering cross section of a particle, one could find the scattered transmittance per unit incident intensity, I_0, as [8]:

$$\frac{I_{transmitted}}{I_0} = \exp(-C_{sca}) \tag{17}$$

Finally, we find the scattered in unit incident intensity as:

$$\frac{I_{sca}}{I_0} = 1 - \frac{I_{transmitted}}{I_0} = 1 - \exp(-C_{sca}) \tag{18}$$

Common difficulties with Mie theory. Mie theory, even though it was developed in 1908, was not practically useful until the advent of computers in the late 1960's. At that time, the first Mie algorithms were developed [12]. Even today, Mie theory calculations are

very tedious and require an excess of computation time. It is not practical to run Mie simulations for very large data sets.

Mie algorithms have been developed in almost every computer language: FORTRAN [11], C++ [13], and MATLAB [14]. While increased computer capacity and speed allows the simulations run much faster, Mie calculations still require long computation times and extensive processor space.

Calculation of the angular eigenfunctions, equations (11) and (12), represents a majority of the time required for Mie calculations. The computation is performed over the entire scattering region, from 0 to 2π. The time will obviously vary depending on the sensitivity you want to achieve, but it is important to include enough steps to achieve a representative result.

A major problem in initial attempts at using Mie theory to describe scattered fields was that most of the formulas for Mie scattering involve infinite sums (i.e., S_1 and S_1). In order to find the point of convergence, many methods have been applied. The first Mie algorithms stopped convergence when $(|a_n|^2 + |b_n|^2)$ fell below (10^{-14}) [12]. Wiscombe approached this problem by obtaining a large amount of data under a convergence condition similar to Dave's and then fit the data to find the number of n terms for convergence[15]. They found that:

$$n = n_{\max} = x + 4.05 \cdot x^{\frac{1}{3}} + 2 \tag{19}$$

For this reason, the angular scattering amplitudes will be calculated as a sum from n=1 to $n_{\max}$ instead of the infinite series in (13) and (14). This was an important finding in that it helped to reduce computation time at a time when computer resources were at a minimum. Even today it greatly improves computational efficiency while maintaining

data integrity.

Size effects. It is useful to understand the significance of polydispersity observed in small particles since it plays such a major role multiple particle TIRM experiments.

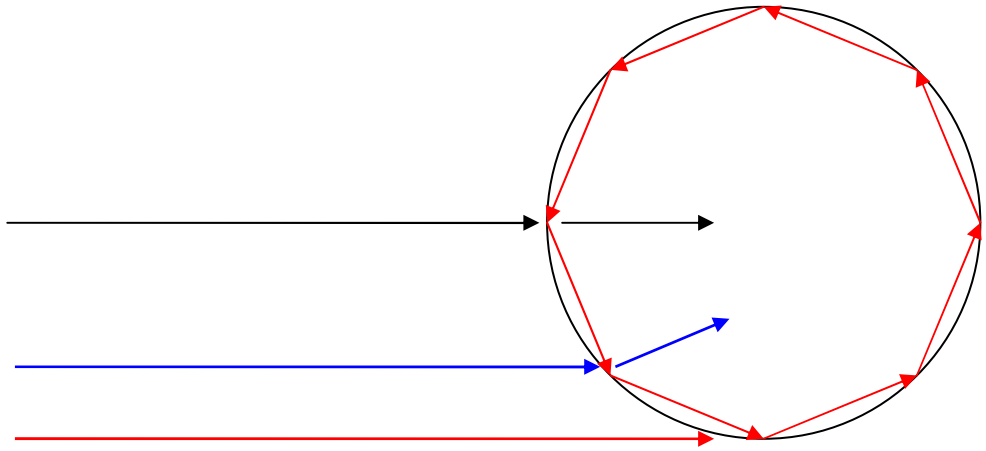

Fig. 6. Description of morphology dependent modes. Plane wave interaction with a spherical particle with $m_{sphere} > m_{medium}$ for light entering at different points on the sphere. Black line (top) is normal incidence. Red line (bottom line) shows light coupling into the sphere and creating an MDR.

In stuck particle experiments (where the baseline intensity is determined) some colloidal particles exhibit intensities that are up to 10 times larger than others. This phenomenon can be explained by the dependence on size and relative refractive index. The refractive index is important because it defines the interaction of the light wave with particle. Snell's Law defines this interaction. If we imagine a plane wave interacting with a spherical surface (see Figure 6) we can see the effects at different points along the surface of the sphere.

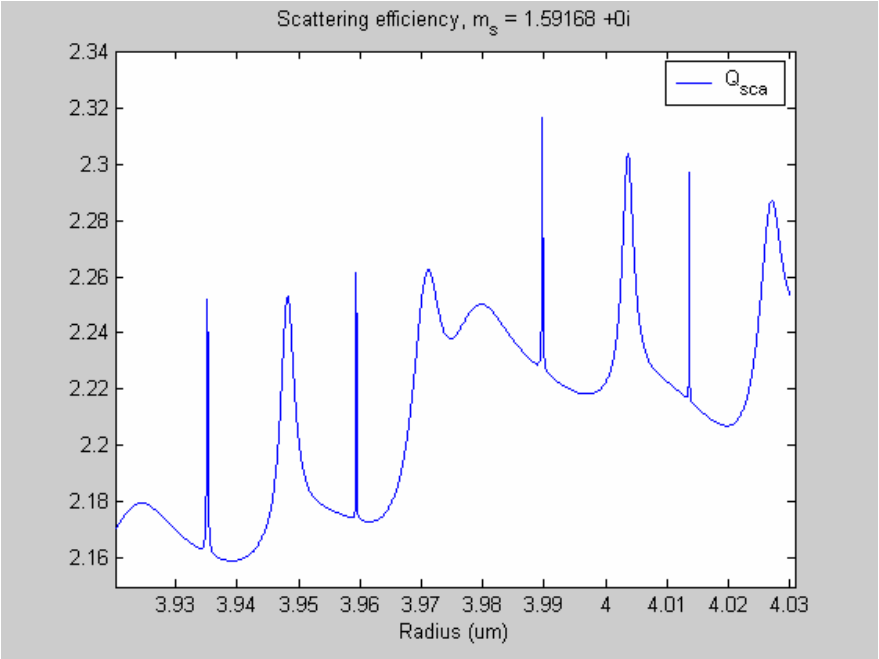

Fig. 7. Q_{sca} for polystyrene spheres in air. Mie scattering efficiency for polystyrene microspheres in air ($m_{medium} = 1.0$) at $\lambda = 488$nm

The red line shows the light coupling into the sphere and the creation of a morphology dependent resonant mode (MDR) or whispering gallery mode (WGM). WGMs have been noticed for some time[16] in spheres, disks and rods. We can see that the MDR modes are highly dependent on the exact size of the particle. The energy circulates near the boundary of the particle in a small mode volume and is confined through total internal reflection. A whispering gallery mode occurs when the light, confined by total internal reflection, circulates the sphere and comes back to the exact point where the light entered the sphere, see the red lines in Figure 6. At this point an amplification of the scattered light occurs and the WGM effects can be physically observed by looking at the scattering efficiency values (Figure 7). Hence, for spherical particles, the resultant cavity confinement is highly dependent on the size of spheres and the relative refractive index.

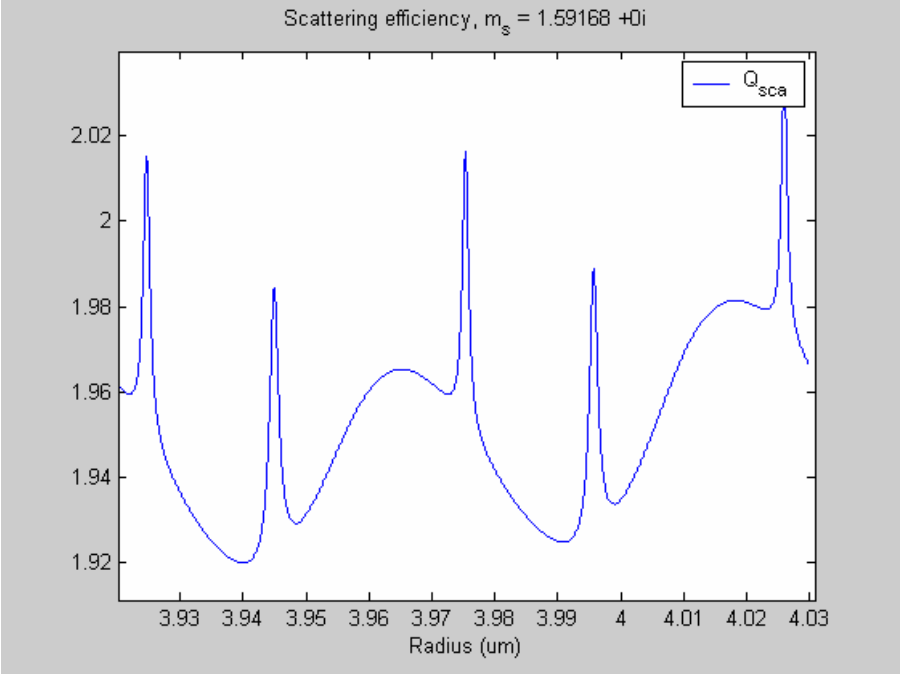

Fig. 8. Q_{sca} for polystyrene spheres in water. Mie scattering efficiency for polystyrene microspheres in air ($m_{medium} = 1.33$) at $\lambda = 488$nm

Since we are interesting in spherical particles, we can use established Mie theory to differentiate the resonant modes. Figure 7 shows the scattering efficiency for polystyrene microspheres in air with radius ranging from 3.93 to 4.02 μm. We observe the resonant modes (sharp peaks) at approximately 3.935, 3.960, 3.99 and 4.015 μm. These modes have been utilized in larger spheres (>100μm) to detect protein absorption on the surface of the spheres[17, 18, 19]. Larger spheres have increased confinement and are easier to couple light into the sphere. In this case, the light is coupled into the sphere by attaching the sphere to an eroded optical fiber. Woggon *et al* have coupled light into the sphere by absorbing quantum dots into or onto the surface of the sphere. They provide a concept for a quantum-dot microlaser in the visible range with this work[20].

If we look at spherical particles suspended in water, which is the case for TIRM, we can see that the energy is much less confined (Figure 8). We do not see the very fine

resonant peaks associated with high cavity confinement. As discussed, the reduced value of the relative refractive index results in the reduced confinement. The confinement is dependent on the relative refractive index as well as the size of the particle, hence they are known as morphology dependent modes. We see that as the relative refractive index increases, confinement increases and WGMs are observed at smaller particle sizes. Generally, we observe confinement increase (see more resonant peaks) as relative refractive index increases or as particle size increases (Figure 9). As we discussed, Mie theory calculations are highly dependent on the relative refractive index and the size parameter, x. A small change in either parameter may result in large changes in scattered light characteristics.

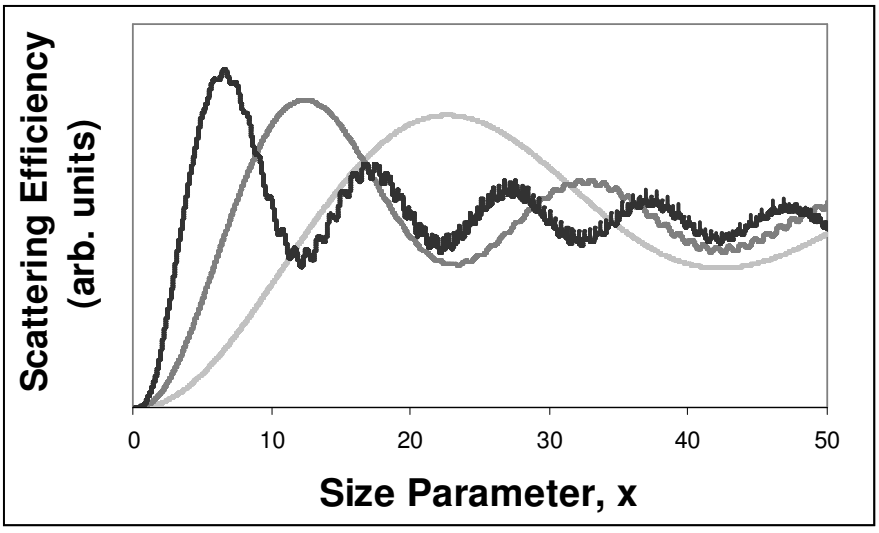

Fig. 9. Q_{sca} for polystyrene spheres in various mediums. Scattering efficiency for microspheres in a medium with an index of refraction of 1.33. Microspheres are taken to have an index of refraction of 1.45 (light grey), 1.55 (dark grey) and 1.75 (black).

We now see how particle polydispersity can be so detrimental to multiple particle TIRM experiments. 4μm polystyrene microspheres ordered from Interfacial Dynamics

are reported to have a coefficient of variation of 5.1% and a standard deviation of 0.2μm. This means that microspheres used for multiple particle TIRM experiments can range from approximately 3.4μm to 4.6μm. This distribution will result in a wide range of baseline intensity values. The resulting distributions are shown in the **Results and Discussion** section.

MATLAB code for Mie theory. In order to achieve our goal of modeling scattered intensities for multiple particle TIRM studies, we had to create a computer model that would calculate the above Mie scattered intensities. There are many who have previously developed code for Mie theory on various platforms. Since I have had the most experience with MATLAB, this seemed a logical choice for a place to start. For the code I relied heavily on Bohren and Huffman for background and theory surrounding Mie scattering. A MATLAB code previously written by Christian Mätzler[14] provided a good reference for many of the programs that were developed. I have included my programs in APPENDIX A for reference.

The program adam_angles.m (Appendix A.1) is used to calculate the scattered efficiency, cross-section and intensity for unpolarized, perpendicular and parallel polarized light. In this program, we use Mie theory to calculate scattered intensities for certain parameters. These parameters include:

- lam - the wavelength of the incident light, λ
- m_sphere – complex refractive index of the sphere
- m_medium – the complex refractive index of the medium surrounding the sphere
- r_median – the expected median radius value of the spheres in question (e.g. r_median = 3e-6 for nominal 6 μm spheres)
- x_steps – the number of steps in x (normally use 1500)
- theta_steps – the number steps in the full 2π radian circle (normally use 4001)

- r_beg – beginning value for the range of sphere sizes of interest
- r_end – last value for the range of sphere sizes of interest
- NA – the numerical aperture value for the microscope used in experiments

The program calculates the angular scattering amplitudes (S_1 and S_2) within the cone of observation defined by the numerical aperture of the microscope (N.A.). Once the scattering amplitudes are defined we use equations (15), (16) or (18) to calculate the variables of interest; C_{sca}, Q_{sca}, or I_{sca}. In calculation of C_{sca} we normalize the value in order to observe the values more straightforwardly.

Since the refractive index of polystyrene is vital to accurate calculations, the exact value is needed. Research has shown that the exact index of refraction of polystyrene can be found as a function of the incident wavelength. With λ in units of micrometers we find the exact value as [21]:

$$m_{polystyrene} = 1.5725 + \frac{0.0031080}{\lambda^2} + \frac{0.00034779}{\lambda^4} \tag{20}$$

After running adam_angles.m, we run the program histfn.m (Appendix A.5) to obtain a histogram of normalized frequency of particle size versus normalized intensity. The histfn.m program uses the scattered intensity values obtained by the adam_angles.m program. It requires definition of certain constraints that define the size and log normal distribution of the particles. The parameters that must be defined are:

- d_median – the exact, measured median diameter value of the spheres being used experimentally
- logn_s – this parameter describes the width of the log normal distribution centered at d_median
- bins – the number of bins for the histogram that is produced
- pol – polarization of the incident light; pol = 1 for perpendicular polarization, pol = 2 for parallel polarization, and pol = 3 for unpolarized light

Studies of levitated colloidal systems have shown that particle polydispersity follows a log normal distribution[22]. We apply a log normal distribution using the following equation:

$$\text{logn} = \exp\left(-\frac{1}{2} \cdot \left[\frac{\log\left(\frac{\text{d}}{\text{d\_median}} \right)}{\text{logn\_s}} \right]^2 \right) \tag{21}$$

Normally, logn_s = 0.073 for our model. d is the diameter of the particle defined over the range [2*r_beg – 2*r_end] with "x_steps" number of data points.

The histfn.m program works by dividing the intensity distribution into bins that are equally spaced. The exact intensity values are recorded for each bin in a variable (Isca_NA_hist) wherein each column is representative of one bin. The corresponding size values are then recorded (variable x_hist). We use radius values to calculate the number of particles in each bin according to the log normal distribution described by equation (21). The frequency, or number, of particles is then normalized to the largest value. The intensity found at the center of each bin is also normalized to the largest value. We can observe the intensity distributions for a given range of microspheres by looking at the normalized intensities versus the normalized frequency (or normalized number of particles).

The output of the histfn.m program is two figures. The first is a graph of normalized intensity versus normalized particle frequency. The second is both the intensity distribution and the log normal distribution versus particle radius.

We also have created a program used to observe scattered intensity distributions

in all directions. The program adam_angplots.m (Appendix A.6) allows us to look at the intensities of perpendicular and parallel polarizations in a polar plot. For example, we saw the angular scattering plot for a 4μm polystyrene microsphere at λ = 488nm for parallel polarized scattered light (from 0 to π) and perpendicular polarized scattered light (from π to 2π) in Figure (5).

SUMMARY AND CONCLUSIONS

Simulation parameters. Modeling light scattering using Mie is advantageous for many reasons. One of these is that there are very few variables in calculating scattered intensities. Once a laser, microsphere material, and N.A. are chosen experimentally, there is little that will vary in calculating intensities. The refractive indices of water and polystyrene are well defined and the Mie calculations have been studied extensively. The only variables in the simulation are the size range to be tested, the number of steps in scattering angle (θ) and the number of steps in x. This advantageous because there is little room allowed for error to be introduced into the model. Any error in the results will be experimental error. We will discuss the reasons for this error as we discuss the experiments for each size of microsphere.

Chew[5] *et al* have shown that basic Mie theory can be used to model evanescent scattering but only under the assumptions that 1) the evanescent wave is generated by incident light that is perpendicularly polarized and 2) the detection plane is located at a scattering angle of 90º. The experimental set-up was designed around these parameters. These stipulations restrict the amount of experimental data that we could use to compare to Mie theory. The Argon Ion laser (488nm) emits parallel polarized light so we used two mirrors to shift the polarization to perpendicular polarization. Other lasers used for DCPM by Dr. Bevan's group include a 632.5 nm laser and a 543 nm laser. Both emit unpolarized light and are thus not viable for comparison with our Mie theory calculations.

The parameters that define the histogram have the greatest impact on the presentation of the model information. Accurately choosing value for median diameter, number of bins and width of the log normal distribution is very important. We can

change these values to reduce error in the model. Thus, it is very important that we use the true experimental median diameter. Also, for the bin number and log normal width, we must be consistent in each experiment. The width of the log normal distribution remains the same for each simulation. The value defining this parameter was set to logn_s = 0.073. Since we have 1500 data points for each experiment, we choose to use 50 bins for each experiment. Choices for the median diameter will be discussed for each microsphere size. Changes in these parameters will alter the position of the fine structure peaks while maintaining the general distribution.

We use the Mie theory model described previously to observe scattered intensity values for 1, 4 and 6μm polystyrene microspheres. Each simulation is run for polystyrene microspheres in water the following parameters:

- λ = 488nm
- polarization = perpendicular
- x_steps = 1500
- theta_steps = 4001
- N.A. = 0.60 (40x magnification)

The histogram for the log normal distribution is obtained using 50 bins and logn_s = 0.073 to define the width of the distribution. The median diameter values for each set of experiments were attained from g(r) and dynamic light scattering (DLS) experiments performed by Hung-Jen Wu in Dr. Bevan's Lab.

It is also important to note that the model we have created has theoretically infinite resolution. We can define the steps in x and θ so that we can resolve any and all resonant peaks for a given size parameter. But, experimentatlly we can not achieve this

resolution. This will account for some of the differences between the experimental and theoretical results.

Experimental methods. Microscope glass slides from Corning (Corning, NY) were used as surfaces in all experiments. glass slide surfaces were initially washed for 30 minutes in Nochromix (Godax Laboratories, Takoma Park, MD) followed by rinsing with double deionized water (DDI) and drying with high purity nitrogen. A 10mm ID x 12 mm OD Viton O-ring (McMaster Carr, Los Angeles, CA) were used as spacers for the sedimentation cells.

1, 4 and 6 μm polystyrene colloids were purchased from Interfacial Dynamics Cooperation (Eugene, OR) and used without further purification. In each experiment, particles were diluted in DI water to obtain bulk particle concentrations that produced desired interfacial concentrations after sedimentation. A custom water purification system using reverse osmosis, deionization, filters, and ultraviolet light treatments was used to produce deionized water with resistivities of 17.2 - 17.4 Ohms/cm. Particle solutions were first placed in the batch cell couple hours for particle sedimentation, and 5M NaCl solution were injected to screen electrostatic repulsive interactions between particle and surfaces to stick particle on glass slides. The particle size distributions were measured using dynamic light scattering (ZetaPALS, Brookhaven Instrument Corporation, Holtsville, NY).

Fig 1a shows a schematic representation of an optical microscope (Axioplan 2, Zeiss, Germany) and CCD camera setup for monitoring evanescent wave scattering from particle ensembles as shown in Fig 1b. An o-ring/cover glass batch sedimentation cell is optically coupled to a 68° dovetail prism (Reynard Corp., CA) using index matching oil

(n=1.515). The prism is mounted on a three point leveling stage. In each experiment, a 40X objective (NA=0.60) was used in conjunction with a 12 bit CCD camera (ORCA-ER, Hamamatsu, Japan) operated with 2x binning to produce a capture rate of 18 frames/sec with 672 x 512 resolution (pixel=304nm and , 204 x 155 μm^2 image size for 40X objective). The evanescent wave was generated using a 150 mW, 488 nm Argon Ion laser (Melles Griot, Carlsbad, CA) to produce an evanescent wave decay length of 88 nm (n_g=1.515, n_w=1.333).

Image analysis algorithms coded in FORTRAN were used to track the lateral locations and integrate the evanescent wave scattering intensity for each particle. Standard video microscopy algorithms were used to locate and track centers of the evanescent wave scattering signal on each particle[23]. The total scattering intensity from each particle was obtained by integrating all pixels within a specified radius of the scattering signal center pixel. The scattering intensities of stuck particle ensembles were measured and averaged in a short period of time. All image analysis was performed using PC's and multi-page TIFF files containing separate images in a single file.

In measurements of two dimensional pair distribution functions, a 100X objective used in conjunction with the 12 bit CCD camera using an image with 1344 x 1024 resolution (60.7 nm pixels).

Results and discussion - 1µm polystyrene particles. The results for 1µm polystyrene microspheres can be seen in Figures 10 and 11 below.

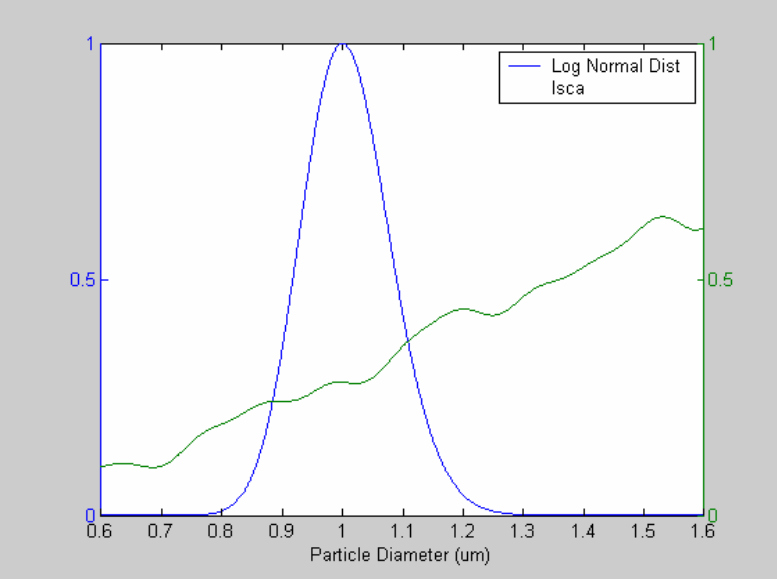

Fig. 10. 1µm polystyrene - Scattered intensity and size distribution vs. radius. Blue is the log normal distribution. Green is the intensity distribution.

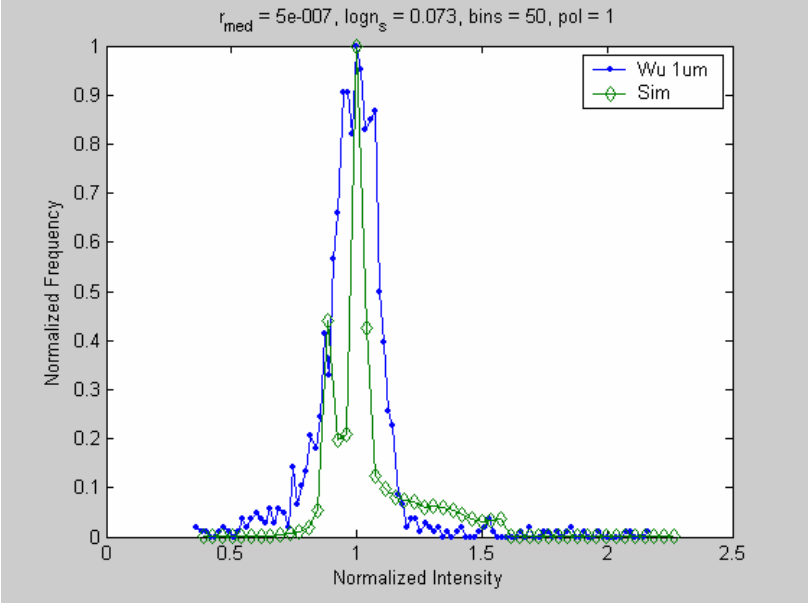

Fig. 11. 1µm polystyrene – Intensity vs. particle frequency. Normalized intensity versus normalized frequency for 1µm polystyrene stuck-particle experiments. Green is simulation results. Blue is the experimental results.

The 1μm intensities show some difference from the experimental intensities. The most notable difference is that we see two large peaks of particle frequency. We can attribute these peaks to an intensity distribution that is not increasing or decreasing consistently over the entire range. For example, if a bin from the histogram contains the intensity values related to sizes ~ 0.97 – 1.07μm (Figure 10) we see an increased frequency of particles. This results in the large, central peak in Figure 11. The smaller peak is the second area of intensities with a large frequency of particles, from ~ 0.85 – 0.93μm.

In the 1μm experiments we can see that the variation in scattered intensity is at a minimum. For small polystyrene spheres suspended in water, the energy is not tightly confined so we do not see the morphology dependent modes associated with higher confinement. Changes in size have less effect for spheres of this size.

Theoretically, this is a good result for DCPM and multiple particle experiments because variations in scattered intensity are smaller. However, noticeable differences are still observed. It is almost impossible to produce an entirely uniform intensity distribution. While size effects are less prominent for 1μm particles, there are other problems encountered.

First of all, establishing the baseline intensity is more difficult with the 1μm particles. Their size and weight make it very difficult to physically attach the spheres to the glass slide. Even when the electrostatic potential is not applied the spheres tend to levitate. It is difficult to determine if the intensity is scattered from stuck-particle or from a levitating particle. For larger spheres, the increased weight of the spheres allows gravity to attach the spheres to the surface.

Another problem is attributed to the very small size of the particles. As mentioned in the experimental section, calculating the total scattered intensity of each particle requires integrating all pixels within a specified radius of the scattering signal center pixel in a short period of time. This work is performed by the computer. The problem with 1μm particles is that the computer sometimes has problems integrating such a small number of pixels. Increased sensitivity of the detection system could be solution for this problem.

Also, we observe that some 1μm particles express intensity values that are greater than the intensity of larger particles. In theory, larger particles will scatter light better and thus be more intense. One answer to this question may be attributed to the decay length of the evanescent wave. The decay length is reported to be 88nm. This height represents 8.8% of the diameter of the 1μm particles. Thus, more light, by proportion is scattered by the sphere. Comparably, the decay length represents only 2.2% of 4μm particles and 1.4% of 6μm particles. Further study is required to verify this theory.

1μm particles are so small that it was not possible to use g(r) or DLS experiments to measure the true median diameter of the particles. For this reason, we assumed a median diameter of 1μm.

Results and discussion - 4µm polystyrene particles. The results for 4µm polystyrene microspheres can be seen in Figures 12 and 13 below.

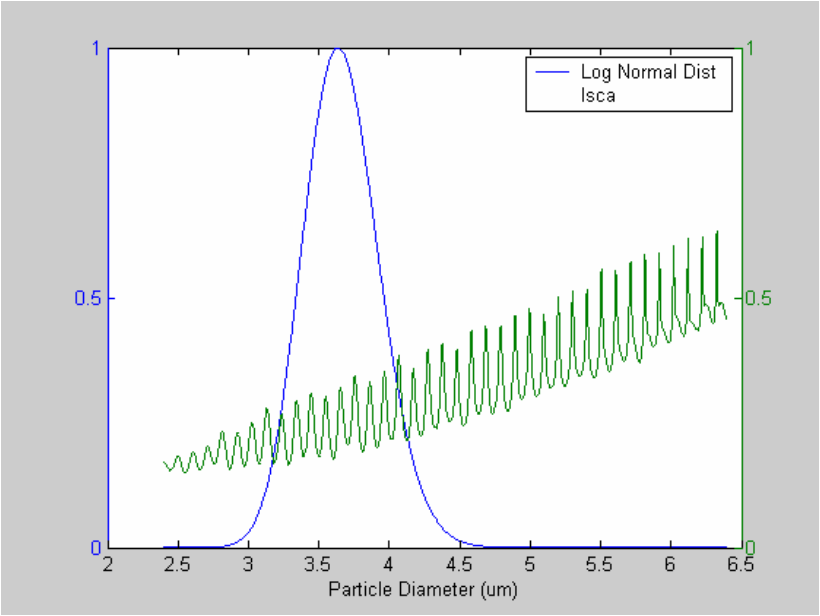

Fig. 12. 4µm polystyrene - Scattered intensity and size distribution vs. radius. Blue is the log normal distribution. Green is the intensity distribution.

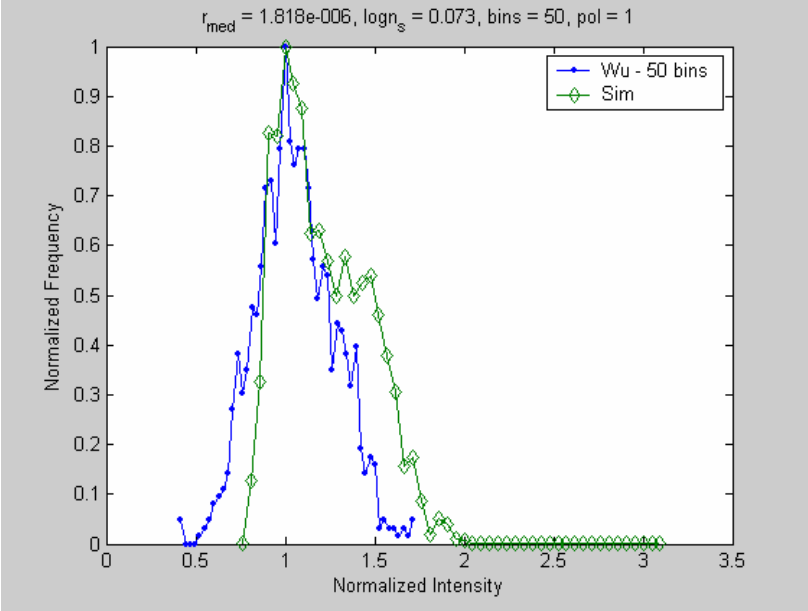

Fig. 13. 4µm polystyrene – Intensity vs. particle frequency. Normalized intensity versus normalized frequency for 4µm polystyrene stuck-particle experiments. Green is the simulation results. Blue is the experimental

The 4μm simulations show a significant variation in scattered intensity while producing results that closely followed the experimental results. g(r) and DLS studies showed that the true median diameter of the 4μm spheres is 3.636μm. Using 50 bins we see the resulting distribution in Figure 13. The general shape of the distribution matches reasonably well but the fine structure peaks are slightly shifted. These peaks can be "manipulated" to produce results that may seem more significant. If we look at the calculated intensity values we see a series of peaks and troughs (Figure 14). If we were to choose the median diameter to lie at the top of a peak we would produce a distribution with fine structure that is considerably different that a distribution with the median diameter chosen to lie in a trough area.

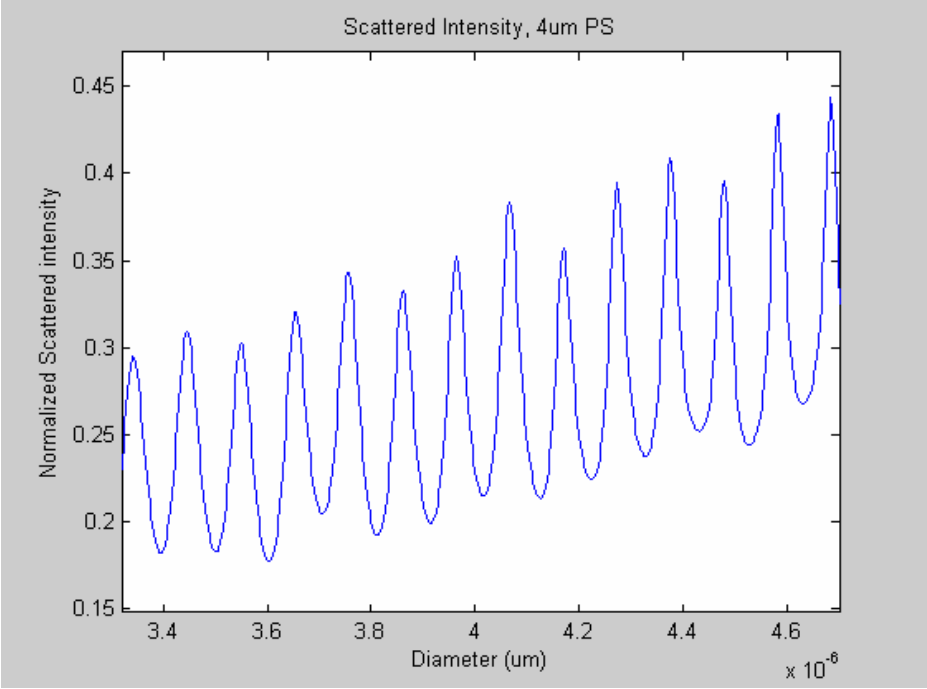

Fig. 14. I_{sca} for 4μm polystyrene – Zoomed in

For example, changing the median diameter from 4.02μm to 4.09μm will shift the center intensity from a normalized value of 0.21 (trough) to 0.375 (peak) (see Figure 14).

There is some discretion to be shown in choosing median diameter values. The experimentally calculated values represent the most likely median value and are thus a good estimation. We can obtain a simulated distribution that more closely follows the experimental distribution if we pick and choose parameter values. Figure 15 was obtained using a median diameter value of 4.2µm.

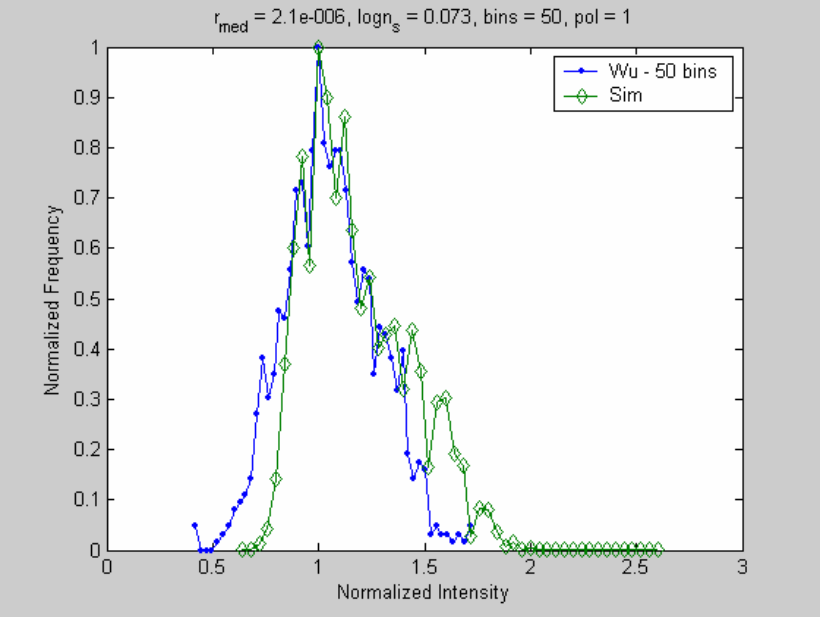

Fig. 15. Effects of changing value of median diameter for 4µm polystyrene. Median diameter = 4.2µm

Results and discussion – 6µm polystyrene particles. The results for 6µm polystyrene microsphere can be seen in Figures 16 and 17 below.

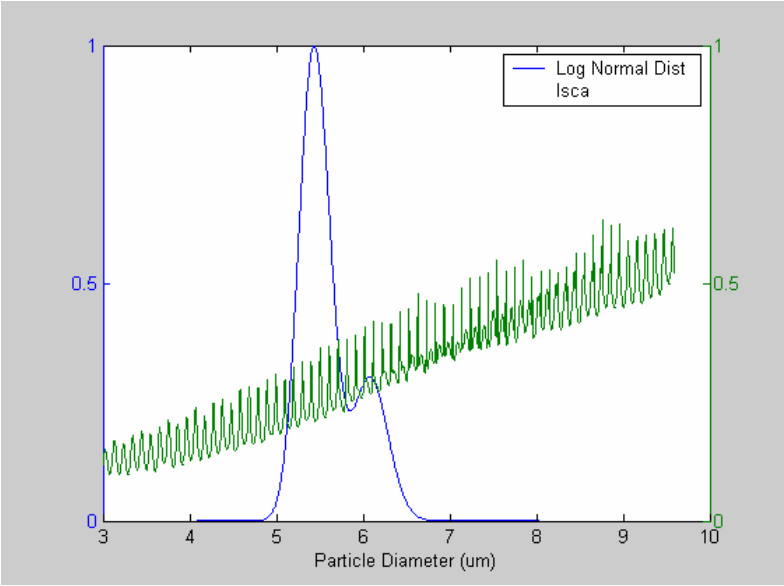

Fig. 16. 6µm polystyrene - Scattered intensity and size distribution vs. radius. Blue is the particle size distribution. Green is the intensity distribution.

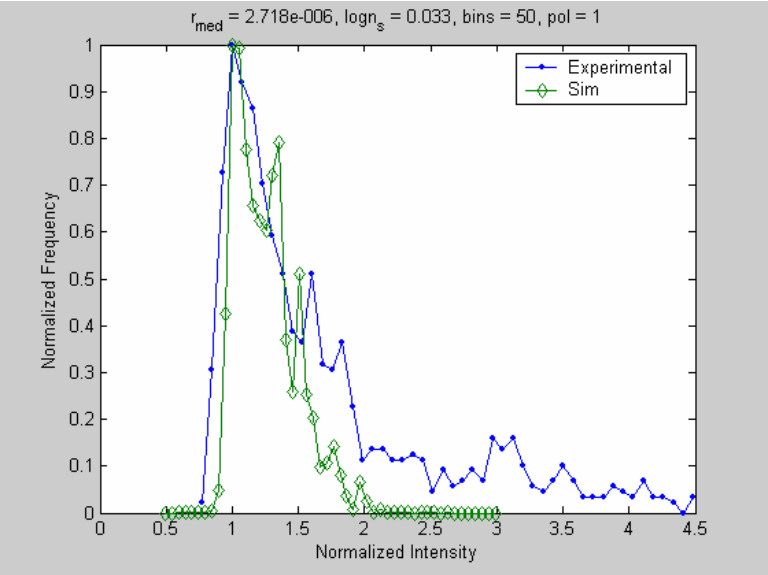

Fig. 17. 6µm polystyrene – Intensity vs. particle frequency. Normalized intensity versus normalized frequency for 6µm polystyrene stuck-particle experiments. Green is the simulation results. Blue is the experimental results.

The 6μm polystyrene particles were of great interest because of the long tail exhibited experimentally (Figure 17). This distribution was very different when compared to the other sizes of polystyrene particles. We see that the simulated distribution fits the experimental results very well. Also, it is evident that the size distribution, obtained through g(r) calculations, is much different than the other particle sizes. g(r) measurements are performed by allowing the particles to come in contact with each other so as to create a single layer of microspheres. As the spheres scatter light, the location of the center of the sphere is recorded. The computer calculates the average distance between spheres and produces a bell shaped curve. The most common median diameter value is represented at the peak of the curve. For the 6μm particles, three peaks were observed. The largest peak represented a median diameter of 5.436μm. This is the value we defined to produce the distribution in Figure 17. The 2nd peak represented a median diameter of 6.084μm. The 3rd was much smaller and had no effect on the simulation results.

The multiple peaks significantly contribute to the abnormal size distribution. Hung-Jen Wu of Dr. Bevan's lab performed these experiments and we discussed this phenomenon as a possible reason for the long tail of the 6μm particles. The smaller peaks represent a less likely estimate of the true median diameter of the particles. The presence of these peaks is evidence of large polydispersity in the 6μm particles, which our model predicts very well.

Summary and conclusion. We have shown that Mie theory can provide an excellent method for studying the behavior of scattered light. Using strictly defined limitations[3] basic Mie theory can be used to model scattering of an evanescent wave by a spherical

particle. This information has allowed for the explanation and study of scattered intensity distributions created by multiple particle TIRM experiments, such as DCPM. By applying Mie theory we can model TIRM intensity distributions for any type of spherical particle that is suspended in an aqueous solution. The incident light is restricted to allow only light that is perpendicularly polarized and that falls within a cone of observation defined by the microscope used experimentally.

An important result of this work is that we have been able to prove what many have suspected since the introduction of TIRM. Recent technological advances have made multiple particle TIRM experiments viable and important to further study. Thus, understanding why these experiments show a large variation in stuck-particle intensity is very important. Then, experimental methods may be designed so that we can make use of the high sensitivity and resolution of TIRM experiments such as DCPM.

The 6μm polystyrene particles, because of their uncharacteristic size distribution, provided the best test for our model. The 4μm particle results best matched the experimental results. Under the conditions described we are able to accurately predict the effects of polydispersity in TIRM experiments. Since our theoretical results match up so well with the experimental results, we conclude that the primary reason for varying scattered intensities in stuck-particle TIRM experiments is particle polydispersity.

The manufacturing process of polystyrene microspheres is likely the largest hindrance in achieving uniformity. It is very difficult to purchase microspheres that will have the absolute smallest variability in particle size. The 1μm polystyrene spheres expressed so many problems that it will not be advantageous to use them in multiple particle TIRM studies. And while the 6μm particles are easier to deal with

experimentally, the polydispersity is too large to achieve accurate results. For this reason, we find that it would be best to use polystyrene microspheres with a median diameter of 4.2μm for DCPM or other multiple particle studies. This distribution will allow for more precise ensemble averaging of potential energy profiles and will generate better results.

Future work. In the future, a more rigorous model of the evanescent wave would be yield results that are more precise. Also, any type of incident light may be studied at a collection angle that is not restricted. This will be useful in modeling varying system parameters and in creating more data for comparison.

For future work, this model will need to be transferred into a computer language that is more efficient that MATLAB. While MATLAB has been very effective, it is very, very slow. Simulations for 1500 data points calculated with 4000 angular steps took approximately eight to ten hours to complete. This is really unacceptable for future work that will no doubt include more complex systems. We chose to use MATLAB mainly because I have had the most experience with the language. A much more efficient code should be written in FORTRAN or C++ in order to minimize calculation times.

REFERENCES

1. D.C. Prieve, Adv. Colloid Int. Sci. **82**, 93 (1999).

2. D.K. Cheng, *Fundamentals of Engineering Electromagnetics* (Prentice Hall, New Jersey, 1993).

3. H. Chew, D.S. Wang, M. Kerker, Applied Optics **18**, 2679 (1979).

4. H.J. Wu, M.A. Bevan, Langmuir **21**, 1244 (2005).

5. M. Kerker, *The Scattering of Light and Other Electromagnetic Radiation* (Academic Press, New York, 1969).

6. G.M. Kepler, S. Fraden, Physics Review Letters **73**, 356 (1994).

7. G. Mie, Ann. Der Physik **25**, 377 (1908).

8. C.F. Bohren, D.R. Huffman, *Absorption and Scattering of Light by Small Particles* (Inerscience, New York, 1983).

9. D.C. Prieve, J.Y. Walz, Applied Optics **32**, 1629 (1993).

10. A.V. Zvyagin, K. Goto, J. Opt. Sci. Am. A **15**, 3003 (1998).

11. P.W. Barber, S.C. Hill, *Light Scattering by Particles: Computational Methods* (World Scientific, New Jersey, 1998).

12. J.V. Dave, IBM J. Research Dev. **302** (May 1969).

13. H. Du, Applied Optics **43**, 1951 (2004).

14. C. Mätzler, MATLAB Functions for Mie Scattering and Absorption (Research report, University of Bern, June 2002).

15. W.J. Wiscombe, Applied Optics **19**, 1505 (1980).

16. P. Chylek, J.T. Kiehl, M.K.W.Ko, Applied Optics **17**, 3019 (1978).

17. I. Teraoka, S. Arnold, F. Vollmer, J. Opt. Soc. Am. B **20**, 1937 (2003).

18. F. Vollmer, D. Braun, A. Libchaber, M. Khoshsima, I. Teraoka, S. Arnold, Applied Physics Letters **80**, 4057 (2002).

19. S. Arnold, M. Khoshsima, I. Teraoka, S. Holler, F. Vollmer, Optics Letters **28**, 272 (2003).

20. M.V. Artemyev, U. Woggon, R. Wannemacher, H. Jaschinski, W. Langbein, Nano Letters **1**, 309 (2001).

21. M. Xiaoyan, J.Q. Lu, R.S. Brock, K.M. Jacobs, P. Yang, X.H. Hu, Phys. Med. Bio. **48**, 4165 (2003).

22. T.O. Pangburn, M.A. Bevan, J. Chem. Phys. **123**, 174904 (2005).

23. J.C. Crocker, D.G. Grier, J. Colloid Int. Sci. **179**, 298 (1996).

APPENDIX A

MATLAB CODE FOR MODELING

A.1 – Scattered intensity – adam_angles.m

A.2 – Scattering amplitudes – adam_s.m

A.3 – Mie coefficients, a_n and b_n – adam_anbn.m

A.4 – Angular coefficients, π_n and τ_n – adam_pi_tau.m

A.5 – Histogram and plotting code – histfn.m

A.6 – Angular plots for scattered intensities – adam_angplots.m

A.1 – adam_angles.m

Angular scattering calculations for scattering efficiency, cross-section and intensity for unpolarized, parallel polarized and perpendicularly polarized light within the cone of detection for a given N.A.

```
% Angular scattering calculations
% clear all;

% Set parameters
lam = 488e-9;
m_sphere_lam = (1.5725)+(0.0031080/((lam*10^6)^2))+(0.00034779/((lam*10^6)^4));
m_sphere = complex(m_sphere_lam,0);
m_medium = complex(1.33,0);
r_median = 3e-6;
x_steps = 1500;
theta_steps = 4001;
m = m_sphere/m_medium;
r_beg = 2.1e-6;
r_end = 4.2e-6;

% NA calculations
NA = 0.60;
NA_ang_radians = asin(NA*1.0/m_medium);
NA_ang_deg = NA_ang_radians*180/pi;
NA_ang_deg1 = (90) - NA_ang_deg;
alpha_ang1 = (NA_ang_deg1)*pi/180;
alpha_ang2 = ((90) + NA_ang_deg)*pi/180;

x_beg = 2*pi*r_beg*m_medium/lam;
x_end = 2*pi*r_end*m_medium/lam;
cnt = 0;
for xcnt = 1:x_steps;
   cnt = cnt+1
   x_step = (x_end - x_beg)/x_steps;
   x(xcnt) = x_beg + (xcnt-1)*x_step;
   nmax = round(2+x(xcnt)+4*x(xcnt).^(1/3));

   theta_steps = theta_steps;
   theta_min = 0;
   theta_max = 2*pi;
   d_theta=(theta_max - theta_min)/(theta_steps-1);
   s_1 = [];
   s_2 = [];
   l = 0;                        %NA angle counter

   for k=1:theta_steps
      theta(k) = theta_min + (k-1)*d_theta;
      mu(k) = cos(theta(k));
      a(:,k)=adam_s(m,x(xcnt),mu(k));
      s_1(k)= a(1,k);
      s_2(k)= a(2,k);
      if (theta(k) > alpha_ang1) && (theta(k) < alpha_ang2)
```

```
        l = l+1;
        s_1_NA(l) = a(1,k);
        s_2_NA(l) = a(2,k);
      end
    end

    i_perp = abs(s_1).^2;          % Scat irradiance per unit incident irradiance (perp)
    i_par = abs(s_2).^2;           % Scat irradiance per unit incident irradiance (par)
    i_perp_NA = abs(s_1_NA).^2;
    i_par_NA = abs(s_2_NA).^2;

    r(xcnt) = x(xcnt)*lam/(2*pi*m_medium);

    % Unpolarized
    S_perp = i_perp/(pi*(r(xcnt).^2));
    S_par = i_par/(pi*(r(xcnt).^2));
    S_power = S_perp + S_par;
    Qsca_unpol(xcnt) = sum(S_power);
    % NA restricted
    S_perp_NA = i_perp_NA/(pi*(r(xcnt).^2));
    S_par_NA = i_par_NA/(pi*(r(xcnt).^2));
    S_power_NA = S_perp_NA + S_par_NA;
    Qsca_NA_unpol(xcnt) = sum(S_power_NA);
    % Perpendicular polarization only
    Qsca_perp(xcnt) = sum(S_perp);
    Qsca_NA_perp(xcnt) = sum(S_perp_NA);
    % Parallel polarization only
    Qsca_par(xcnt) = sum(S_par);
    Qsca_NA_par(xcnt) = sum(S_par_NA);
end

% Unpolarized
Csca_unpol = Qsca_unpol.*(pi*(r.^2));
Csca_unpol_norm = Csca_unpol/max(Csca_unpol);
Isca_unpol = 1 - exp(-1*Csca_unpol_norm);
% Unpolarized NA restricted
Csca_NA_unpol = Qsca_NA_unpol.*(pi*(r.^2));
Csca_NA_unpol_norm = Csca_NA_unpol/max(Csca_NA_unpol);
Isca_NA_unpol = 1 - exp(-1*Csca_NA_unpol_norm);
% Perpendicular polarized, NA restricted
Csca_NA_perp = Qsca_NA_perp.*(pi*(r.^2));
Csca_NA_perp_norm = Csca_NA_perp/max(Csca_NA_perp);
Isca_NA_perp = 1 - exp(-1*Csca_NA_perp_norm);
% Parallel polarization, NA restricted
Csca_NA_par = Qsca_NA_par.*(pi*(r.^2));
Csca_NA_par_norm = Csca_NA_par/max(Csca_NA_par);
Isca_NA_par = 1 - exp(-1*Csca_NA_par_norm);

m1 = real(m); m2 = imag(m);
r_excel = r';
```

A.2 – adam_s.m

Calculation of the angular scattering amplitudes, S_1 and S_2

```
%  s1 and s2 calculation
function result = adam_s(m,x,mu)
nmax=round(2+x+4*x.^(1/3));

f = adam_anbn(m,x);
a_n = f(:,1)';
b_n = f(:,2)';

g = adam_pi_tau(x,mu);
pi_n = g(:,1)';
tau_n = g(:,2)';

n = 1:nmax;
s12 = ((2.*n+1)./(n.*(n+1)));
s1_all = s12.*(a_n.*pi_n + b_n.*tau_n);
s2_all = s12.*(a_n.*tau_n + b_n.*pi_n);

s1 = sum(s1_all);
s2 = sum(s2_all);

result=[s1;s2];
```

A.3 – adam_anbn.m

Calculation of the Mie coefficients, a_n and b_n (see Matzler for reference – Mie_ab.m)

```
function result = adam_anbn(m,x)

rho=m.*x;
nmax=round(2+x+4*x.^(1/3));
n_start_d=round(max(nmax,abs(rho))+16);
n=(1:nmax); nu = n+0.5;

pcx = sqrt(0.5*pi*x);

psi_n=pcx.*besselj(nu,x);
psi_nx=[sin(x), psi_n(1:nmax-1)];

chi_n=-pcx*bessely(nu,x);
chi_nx=[cos(x), chi_n(1:nmax-1)];

zi_n=psi_n-i*chi_n;
zi_nx=psi_nx-i*chi_nx;

d_start(n_start_d)=0+0i;


for j=n_start_d:-1:2      % Computation of Dn(z) according to (4.89) of B+H (1983)

   d_start(j-1)=j./rho-1/(d_start(j)+j./rho);

end;

D_n=d_start(n);          % Dn(z), n=1 to nmax

da=D_n./m+n./x;
db=m.*D_n+n./x;


an=(da.*psi_n-psi_nx)./(da.*zi_n-zi_nx);
bn=(db.*psi_n-psi_nx)./(db.*zi_n-zi_nx);


result=[an; bn]';
```

A.4 – adam_pi_tau.m

Calculation of the angular functions coefficients, π_n and τ_n

```
%  pi_n and tau_n
function result=adam_pi_tau(x,mu)
nmax=round(2+x+4*x.^(1/3));


for j=3:nmax
   pi_n(1)=1;
   pi_n(2)=3.*mu;

   tau_n(1)=mu;
   tau_n(2)=3*cos(2*acos(mu));

   pi_n_1=((2*j-1)/(j-1)).*mu.*pi_n(j-1);
   pi_n_2=j./(j-1).*pi_n(j-2);
   pi_n(j)=pi_n_1-pi_n_2;

   tau_n_1=j*mu.*pi_n(j);
   tau_n_2=(j+1).*pi_n(j-1);
   tau_n(j)=tau_n_1-tau_n_2;
end

result=[pi_n;tau_n]';
```

A.5 – histfn.m

Histogram function for a log normal size distribution. Includes plotting functions for scattered intensities vs. radius, log normal distribution vs. radius, and normalized particle frequency vs. normalized scattered intensity

```
% Histogram function

clear Isca_NA Qsca_NA r_sized x_sized
clear new_cv bins bin_centers binedges bin_edges ang_sum_NA_hist x_hist r_hist
clear logn_s logn_a logn_exponent logn histbin logn_hist

d_median =
logn_s =
bins =
pol =

% Polaration dependence
if pol == 1;
   Isca_NA = Isca_NA_perp;
   Qsca_NA = Qsca_NA_perp;
elseif pol == 2;
   Isca_NA = Isca_NA_par;
   Qsca_NA = Qsca_NA_par;
elseif pol == 3;
   Isca_NA = Isca_NA_unpol;
   Qsca_NA = Isca_NA_unpol;
end

% Bin intenstiy values
for bincnt = 1:bins
   binstep = (max(Isca_NA)-min(Isca_NA))/(bins);
   bin_edges(bincnt) = min(Isca_NA)+(bincnt*binstep);
end
bin_edges = [min(Isca_NA) bin_edges];
bin_centers_all = bin_edges + (binstep/2);
bin_centers = bin_centers_all(1:bins);

% Histogram function
g = 0;
for bincnt = 1:bins
   for angcnt = 1:x_steps
      if (Isca_NA(angcnt) >= bin_edges(bincnt)) && (Isca_NA(angcnt) <= bin_edges(bincnt+1))
         g=g+1;
         Isca_NA_hist(g,bincnt) = Isca_NA(angcnt);
         x_hist(g,bincnt) = x(angcnt);
      end
   end
end
%ang_sum_NA_hist = [ang_sum_NA_hist; zeros(1,bins-1) bin_edges(bins+1)];
x_hist = [x_hist; zeros(1,(bins)-1) x_end];
r_hist = lam*x_hist/(2*pi*m_medium);
d_hist = 2*r_hist;
```

```
d = 2*r;

% Log Normal Distribution
logn_s = logn_s;
logn_d0 = d_median;
logn_exponent = 0.5*((log(d_hist/logn_d0)/logn_s).^2);
logn = exp(-logn_exponent);
for histcnt = 1:bins
   histbin = logn(:,histcnt);
   logn_hist(histcnt) = nansum(histbin);
end

[max_logn_hist,max_i] = max(logn_hist);
logn_hist_norm = logn_hist/max_logn_hist;
bin_centers_norm = bin_centers/bin_centers(max_i);

bin_centers1 = bin_centers_norm';
logn_hist1 = logn_hist_norm';

%logn_a_plot = 1./(sqrt(2*pi)*(r*10^6)*logn_s);
logn_exponent_plot = 0.5*((log(d/logn_d0)/logn_s).^2);
logn_plot = exp(-logn_exponent_plot);

% Plotting data
load Wu_1um_488.txt
Wu_1um_int = Wu_1um_488(:,1);
Wu_1um_num = Wu_1um_488(:,2);

load Wu_4um_488_50bins.txt
Wu_4um_50_int = Wu_4um_488_50bins(:,1);
Wu_4um_50_num = Wu_4um_488_50bins(:,2);

load Wu_6um_488.txt
Wu_6um_int = Wu_6um_488(:,1);
Wu_6um_num = Wu_6um_488(:,2);

if lam == 488e-9
   if d0 == 1e-6;
      figure
      plot(Wu_1um_int,Wu_1um_num,'.-',bin_centers_norm,logn_hist_norm,'d-')
      xlabel('Normalized Intensity'); ylabel('Normalized Frequency');
      title(sprintf('r_m_e_d = %g, logn_s = %g, bins = %g, pol = %g',r_median,logn_s,bins,pol));
      h = legend('Wu 1um','Sim');
   elseif d0 == 4e-6,
      figure
      plot(Wu_4um_50_int,Wu_4um_50_num,'.-',bin_centers_norm,logn_hist_norm,'d-')
      xlabel('Normalized Intensity'); ylabel('Normalized Frequency');
      title(sprintf('r_m_e_d = %g, logn_s = %g, bins = %g, pol = %g',r_median,logn_s,bins,pol));
      h = legend('Wu - 50 bins','Sim');
   elseif d0 == 6e-6;
      figure
      plot(Wu_6um_int,Wu_6um_num,'.-',bin_centers_norm,logn_hist_norm,'d-')
      xlabel('Normalized Intensity'); ylabel('Normalized Frequency');
      title(sprintf('r_m_e_d = %g, logn_s = %g, bins = %g, pol = %g',r_median,logn_s,bins,pol));
      h = legend('Experimental','Sim');
   else
```

```
      figure
      plot(bin_centers_norm,logn_hist_norm)
   end
else
   figure
   plot(bin_centers_norm,logn_hist_norm)
end

figure
plotyy(d/(1e-6),logn_plot,d/(1e-6),Isca_NA)
xlabel('Particle Diameter (um)');
h = legend('Log Normal Dist','Isca');
```

A.6 – adam_angplots.m

Angular plots for perpendicular and parallel polarizations

```
%  Angular plots
clear all;

% Set parameters
lam = 488e-9;
m_sphere_lam = (1.5725)+(0.0031080/((lam*10^6)^2))+(0.00034779/((lam*10^6)^4));
m_sphere = complex(m_sphere_lam,0);
m_medium = complex(1.33,0);
m = m_sphere/m_medium;

r = 460e-9;
x = 2*pi*r*m_medium/lam;
x = 50;
nmax=round(2+x+4*x.^(1/3));

% NA calculations
NA = 0.60;
NA_ang_radians = asin(NA*1.0/m_medium);
NA_ang_deg = NA_ang_radians*180/pi;
NA_ang_deg1 = (90) - NA_ang_deg;
alpha_ang1 = (NA_ang_deg1)*pi/180;
alpha_ang2 = ((90) + NA_ang_deg)*pi/180;

theta_steps=3600;
theta_max = 2*pi;
d_theta = theta_max/(theta_steps);

s_1 = [];
s_2 = [];
l = 0;

for k=1:theta_steps
   theta(k) = (k-1)*d_theta;
   mu(k) = cos(theta(k));
   a(:,k)=adam_s(m,x,mu(k));
   s_1(k)= a(1,k);
   s_2(k)= a(2,k);
   if (theta(k) > alpha_ang1) && (theta(k) < alpha_ang2)
         l = l+1;
         s_1_NA(l) = a(1,k);
         s_2_NA(l) = a(2,k);
   end
end

i_perp = abs(s_1).^2;
i_par = abs(s_2).^2;
i_perp_NA = abs(s_1_NA).^2;
i_par_NA = abs(s_2_NA).^2;

m1 = real(m); m2 = imag(m);
```

```
figure
semilogy(theta*180/pi,i_par,theta*180/pi,i_perp,'m')
title(sprintf('Angular Scattering, m = %g + %gi, x = %g',m1,m2,x))
h = legend('I_p_a_r','I_p_e_r_p');

theta_par = theta(1:theta_steps/2);
theta_perp = theta((theta_steps/2)+1:theta_steps);

figure
polar(theta_par,i_par(1:theta_steps/2))
title(sprintf('Angular Scattering, m = %g + %gi, x = %g',m1,m2,x))
hold on
polar(theta_perp,i_perp((theta_steps/2)+1:theta_steps),'m');
legend('I_p_a_r','I_p_e_r_p');
```

VITA

Name:	Adam L. Allen
Address:	337 Zachry Engineering Center 3120 TAMU College Station, TX 77843-3120
Email Address:	adamallen04@yahoo.com
Education:	B.S. Electrical Engineering, Texas A&M University, Aug. 2004. M.S. Biomedical Engineering, Texas A&M University, Aug. 2006